PML Absorbing Boundary Conditions for the Characterization of Open Microwave Circuit Components Using Multiresolution Time-Domain Techniques (MRTD)

Emmanouil M. Tentzeris, *Member, IEEE*, Robert L. Robertson, James F. Harvey, *Member, IEEE*, and Linda P. B. Katehi, *Fellow, IEEE*

***Abstract*—The recently developed multiresolution time-domain technique (MRTD) is applied to the modeling of open microwave circuit problems. Open boundaries are simulated by the use of a novel formulation of the perfect matching layer (PML) absorber. PML is modeled both in split and nonsplit forms and can be brought right on the surface of the planar components. The applicability of the MRTD technique to complex geometries with high efficiency and accuracy in computing the fields at discontinuities is demonstrated through extensive comparisons to conventional finite difference time domain (FDTD). In addition, the numerical reflectivity of the PML absorber is investigated for a variety of cell sizes, some of which are very close to the Nyquist limit ($\lambda/2$).**

***Index Terms*—Absorbing boundary conditions, electromagnetic transient analysis, multiresolution methods, open waveguides, perfectly matched layer.**

I. Introduction

With the advent of microwave circuits used in high-frequency communications, there is a compelling need to develop efficient and reliable full wave simulation techniques for the modeling process. Many practical geometries, especially in circuits and antennas, have been left untreated due to their complexity and the inability of the existing techniques to deal with requirements for large size and high resolution. Recently, the Battle–Lemarie based multiresolution time-domain (MRTD) technique has been successfully applied [1]–[3] to a variety of microwave problems and has demonstrated unparalleled properties. In addition to significant savings in time and in memory by one and two orders of magnitude, respectively, the most important advantage of this new technique is its capability to provide space and time adaptive meshing [4] without the problems encountered by the conventional finite-difference time-domain (FDTD) technique. As a result, MRTD has proven itself to be a powerful technique for electromagnetic computations.

Nevertheless, it is well known that for all discrete-space full wave techniques a special treatment should be given to geometries of interest defined in "open" regions where the computational grid is unbounded in one or more directions. Since the computational domain is limited in space by storage limitations, an appropriate boundary condition should be implemented to effectively simulate open space and satisfy the radiation condition. This boundary condition should have the capability to suppress numerical reflections of the outgoing waves in an almost uniform way for the widest possible frequency range. Field values at the absorbing boundary condition's (ABC) area cannot be calculated by direct application of Maxwell's curl equations due to the fact that the finite differences/summations contain field values at least at points one-half cell outside of the computational plane.

In 1994, Berenger [5] proposed the perfectly matched layer (PML) absorber, which is based upon splitting the E- and H-field components in the ABC area and assigning artificial electric and magnetic loss coefficients. On the condition that these loss coefficients satisfy the PML relationship for each point of the absorber area, this nonphysical absorbing medium has a wave impedance less sensitive to the angle of incidence and frequency of outgoing waves than the pre-existing absorbers. It has been reported that Berenger's PML has provided spurious reflections below -70 dB for a wide range of incidence angles and frequencies. In this paper, the PML principle has been extended to two-dimensional (2-D) MRTD algorithms. The split and nonsplit formulations are presented and reflection coefficients even below -100 dB are demonstrated. The numerical performance of this absorber is investigated for 4–32 cells and for different cell sizes ($\lambda/10$–$\lambda/2.5$). Specifically, propagation constant, characteristic impedance, and field patterns are derived for open transmission lines and compared to 2-D results. In addition, results for a three-dimensional (3-D) patch antenna geometry prove the applicability of the PML to 3-D geometries.

II. Application of PML Absorber to MRTD Technique

In this section, the nonsplit and split extensions of the PML absorber for the Battle–Lemarie MRTD are discussed and their

Manuscript received April 6, 1998; revised May 24, 1999. This work was supported by the U.S. Army Research Office and ARL/Sanders.

E. M. Tentzeris is with the ECE School, Georgia Institute of Technology, Atlanta, GA 30332-0250 USA.

R. L. Robertson and L. P. B. Katehi are with the Radiation Laboratory, Department of Electrical Engineering and Computer Science, University of Michigan, Ann Arbor, MI 48109-2122 USA.

J. F. Harvey is with the Army Research Office, Research Triangle Park, NC 27709-2211 USA.

Publisher Item Identifier S 0018-926X(99)09386-2.

performance is validated for 2-D geometries. Assuming that the PML area is characterized by (ϵ_o, μ_o) and electric and magnetic conductivities $(\sigma_{\rm E}, \sigma_{\rm H})$, the TM^z equations can be written as

$$\epsilon_o \frac{\partial E_x}{\partial t} + \sigma_E E_x = -\frac{\partial H_y}{\partial z} \tag{1}$$

$$\epsilon_o \frac{\partial E_z}{\partial t} + \sigma_E E_z = \frac{\partial H_y}{\partial x} \tag{2}$$

$$\mu_o \frac{\partial H_y}{\partial t} + \sigma_H H_y = \frac{\partial E_z}{\partial x} - \frac{\partial E_x}{\partial z}. \tag{3}$$

Without loss of generality, PML cells only along the z direction are considered. The extension to the x and y directions is straightforward. For each point z of the PML area, the magnetic conductivity σ_H needs to be chosen as [5]

$$\frac{\sigma_E(z)}{\epsilon_o} = \frac{\sigma_H(z)}{\mu_o} \tag{4}$$

for a perfect absorption of the outgoing waves. A parabolic spatial distribution of $\sigma_{E,H}$

$$\sigma_{E,H}(z) = \sigma_{E,H}^{\max}\left(1 - \frac{z}{\delta}\right)^p, \text{ with } p = 2 \text{ for } 0 \le z \le \delta \tag{5}$$

is used in the simulations, though higher order distributions (e.g., cubic $p = 3$) can give similar results. The PML area is terminated with a PEC and usually has a thickness varying between 4–16 cells. The maximum value $\sigma_E^{\max}$ is determined by the designated reflection coefficient R at normal incidence, which is given by the relationship

$$R = \exp -\frac{2}{\epsilon_o c}\int_o^\delta \sigma_E(z)\,dz = \exp -(2\sigma_E^{\max}\delta/\epsilon_o c(p+1)). \tag{6}$$

In MRTD, the PML area can be modeled by discretizing the above equations in a similar way to the nonconductive area described in the previous section. Split and nonsplit formulations can be derived as following.

Similarly, the PML equations for the TE^z can be written as

$$\mu_o \frac{\partial H_x}{\partial t} + \sigma_H H_x = \frac{\partial E_y}{\partial z} \tag{7}$$

$$\mu_o \frac{\partial H_z}{\partial t} + \sigma_H H_z = -\frac{\partial E_y}{\partial x} \tag{8}$$

$$\epsilon_o \frac{\partial E_y}{\partial t} + \sigma_E E_y = -\frac{\partial H_z}{\partial x} + \frac{\partial H_x}{\partial z}. \tag{9}$$

A. Split Formulation

Following the approach of [5], H_y is split in two subcomponents H_{yx}, H_{yz} and (1)–(3) are written as

$$\epsilon_o \frac{\partial E_x}{\partial t} + \sigma_E(z) E_x = -\frac{\partial H_{yx} + H_{yz}}{\partial z} \tag{10}$$

$$\epsilon_o \frac{\partial E_z}{\partial t} = \frac{\partial H_{yx} + H_{yz}}{\partial x} \tag{11}$$

$$\mu_o \frac{\partial H_{yx}}{\partial t} = \frac{\partial E_z}{\partial x} \tag{12}$$

$$\mu_o \frac{\partial H_{yz}}{\partial t} + \sigma_H(z) H_{yz} = -\frac{\partial E_x}{\partial z}. \tag{13}$$

For the sake of simplicity in the presentation and without loss of generality, the fields E_x, E_z, H_{yx}, H_{yz} are expanded in terms of scaling functions only in space domain and pulse functions in time domain. By applying Galerkin's technique [1], [2], the following split PML equations are obtained:

$$\begin{aligned}
&{}_{k+1}E^{x,\phi\phi}_{l+1/2,m} \\
&\quad = e^{-\sigma_E^m \Delta t/\epsilon_o}\,{}_kE^{x,\phi\phi}_{l+1/2,m} + \frac{1}{\Delta z\,\sigma_E^m}\left(e^{-\sigma_E^m \Delta t/\epsilon_o} - 1\right) \\
&\qquad \cdot \sum_{i'=m-9}^{m+8} a(i') \\
&\qquad \cdot \left({}_{k+1/2}H^{yx,\phi\phi}_{l+1/2,i'+1/2} + {}_{k+1/2}H^{yz,\phi\phi}_{l+1/2,i'+1/2}\right) \\
&{}_{k+1}E^{z,\phi\phi}_{l,m+1/2} \\
&\quad = {}_kE^{yx,\phi\phi}_{l,m+1/2} + \frac{\Delta t}{\epsilon_o \Delta x}\left(\sum_{i'=l-9}^{l+8} a(i')\right) \\
&\qquad \cdot \left({}_{k+1/2}H^{yx,\phi\phi}_{i'+1/2,m+1/2} + {}_{k+1/2}H^{yz,\phi\phi}_{i'+1/2,m+1/2}\right) \\
&{}_{k+1/2}H^{yx,\phi\phi}_{l+1/2,m+1/2} \\
&\quad = {}_{k-1/2}H^{yx,\phi\phi}_{l+1/2,m+1/2} + \frac{\Delta t}{\mu_o \Delta x} \\
&\qquad \cdot \left(\sum_{i'=l-9}^{l+8} a(i')\,{}_kE^{z,\phi\phi}_{i',m+1/2}\right) \\
&{}_{k+1/2}H^{yz,\phi\phi}_{l+1/2,m+1/2} \\
&\quad = e^{-\sigma_H^{m+1/2}\Delta t/\mu_o}\,{}_{k-1/2}H^{y,\phi\phi}_{l+1/2,m+1/2} \\
&\qquad + \frac{1}{\Delta z\,\sigma_H^{m+1/2}}\left(e^{-\sigma_H^{m+1/2}\Delta t/\mu_o} - 1\right) \\
&\qquad \cdot \sum_{i'=m-9}^{m+8} a(i')\,{}_kE^{x,\phi\phi}_{l+1/2,i'}.
\end{aligned} \tag{14}$$

Exponential time stepping is being used for the field components affected by the PML conductivities σ_E, σ_H. Due to the entire domain nature of the Battle–Lemarie scaling functions, the PML conductivity must be sampled by them over at least 12 cells (six cells per side),

$$\sigma_{E,H}^m = \int_{m-6}^{m+6} \sigma_{E,H}(z)\phi_m(z)\,dz. \tag{15}$$

Similar discretization is used when one or more wavelet resolutions are included. The spatial conductivity is sampled with the appropriate wavelet function in order to provide the conductivity coefficients of the wavelet terms in the MRTD generalized summations. Image theory is applied to extend the conductivity layer outside the terminating PEC's. The presented split formulation follows the idea introduced by Berenger [5] for the FDTD. Nevertheless, an efficient nonsplit form of the PML equations does not demand extra memory for the storage of two H_y subcomponents per cell.

B. Nonsplit Formulation

Substituting in (1)–(3) [3]

$$E_i(x, z, t) = \tilde{E}_i(x, z, t)e^{-\sigma_E(z)t/\epsilon_o} \tag{16}$$

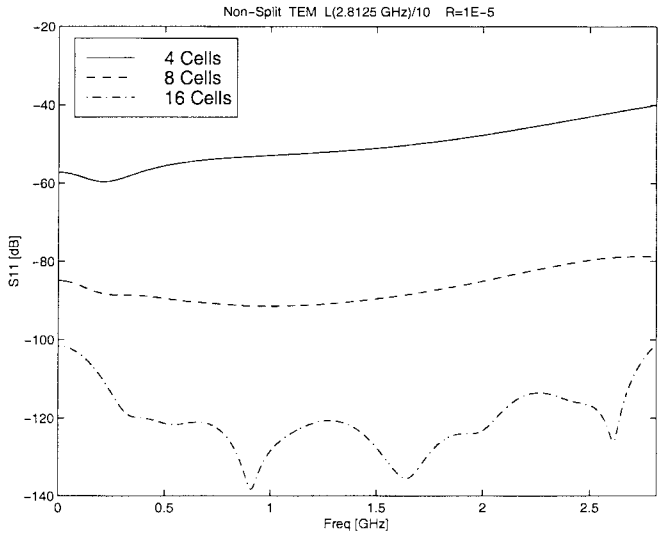

Fig. 1. TEM propagation—dense grid.

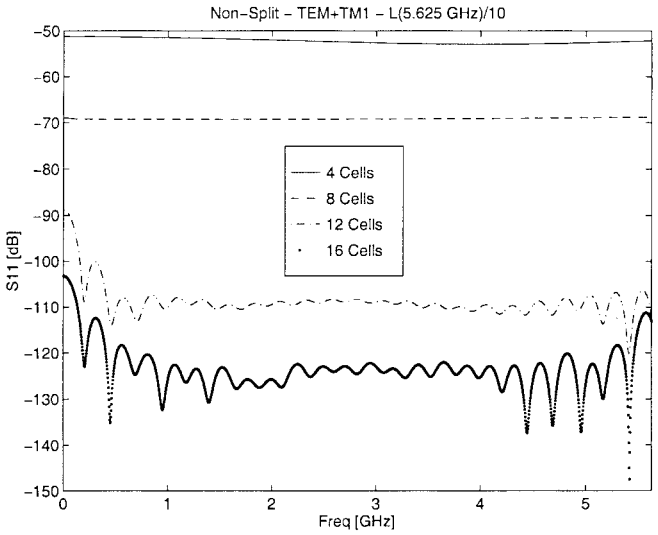

Fig. 2. Multimodal propagation—dense grid.

and

$$H_j(x, z, t) = \tilde{H}_j(x, z, t)e^{-\sigma_H(z)t/\mu_o} \tag{17}$$

for $i = x, z$ and $j = y$ leads to the following system of equations:

$$\epsilon_o \frac{\partial \tilde{E}_x}{\partial t} = -\frac{\partial \tilde{H}_y}{\partial z} \tag{18}$$

$$\epsilon_o \frac{\partial \tilde{E}_z}{\partial t} = \frac{\partial \tilde{H}_y}{\partial x} \tag{19}$$

$$\mu_o \frac{\partial \tilde{H}_y}{\partial t} = \frac{\partial \tilde{E}_z}{\partial x} - \frac{\partial \tilde{E}_x}{\partial z}. \tag{20}$$

Discretizing (18)–(20) and inserting (16) and (17) yields the unsplit formulation of the fields for the PML region

$$\begin{aligned}
&{}_{k+1}E^{x,\phi\phi}_{l+1/2,\,m} \\
&\quad = e^{-\sigma_E^m \Delta t/\epsilon_o}\,{}_kE^{x,\phi\phi}_{l+1/2,\,m} - e^{-0.5\sigma_E^m \Delta t/\epsilon_o}\,\frac{\Delta t}{\epsilon_o} \\
&\qquad \cdot \left(\frac{1}{\Delta z}\sum_{i'=m-9}^{m+8} a(i')_{k+1/2}\,H^{y,\phi\phi}_{l+1/2,\,i'+1/2}\right) \\
&{}_{k+1}E^{z,\phi\phi}_{l,\,m+1/2} \\
&\quad = e^{-\sigma_E^{m+1/2} \Delta t/\epsilon_o}\,{}_kE^{z,\phi\phi}_{l,\,m+1/2} + e^{-0.5\sigma_E^{m+1/2} \Delta t/\epsilon_o}\,\frac{\Delta t}{\epsilon_o} \\
&\qquad \cdot \left(\frac{1}{\Delta x}\sum_{i'=l-9}^{l+8} a(i')_{k+1/2}\,H^{y,\phi\phi}_{i'+1/2,\,m+1/2}\right) \\
&{}_{k+1/2}H^{y,\phi\phi}_{l+1/2,\,m+1/2} \\
&\quad = e^{-\sigma_H^{m+1/2} \Delta t/\mu_o}\,{}_{k-1/2}H^{y,\phi\phi}_{l+1/2,\,m+1/2} \\
&\qquad + e^{-0.5\sigma_H^{m+1/2} \Delta t/\mu_o}\,\frac{\Delta t}{\mu_o}\left(\frac{1}{\Delta x}\sum_{i'=l-9}^{l+8} a(i')_k\right. \\
&\qquad \left. \cdot E^{z,\phi\phi}_{i',\,m+1/2} - \frac{1}{\Delta z}\sum_{i'=m-9}^{m+8} a(i')_k\,E^{x,\phi\phi}_{l+1/2,\,i'}\right)
\end{aligned} \tag{21}$$

where the terms $\sigma^m_{E,H}$ are given by (15).

III. Validation of the PML Split and Nonsplit Algorithms

A parallel-plate waveguide of width $d = 48$ mm, terminated at both ends by PML, is used to validate the described algorithm. A TM^z line source with a Gabor time variation is excited close to the one side of the waveguide. The benchmark MRTD solution with no reflections is obtained by simulating the case of a much longer parallel-plate waveguide of the same width to provide a reflection-free observation area for the time interval of interest. A quadratic variation in PML conductivity is assumed for all cases, with maximum theoretical reflection coefficient of 10^{-5} at normal incidence. Two frequency ranges are investigated—$[0,\, 0.9f_c^{\mathrm{TM}_1}]$ (TEM propagation) and $[0,\, 0.9f_c^{\mathrm{TM}_2}]$ (TEM + TM$_1$ propagation)—where $f_c^{\mathrm{TM}_n} = nc/2d = 3.125n$ (GHz) is the cutoff frequency of the TM$_n$ mode. The time step is chosen to be 0.637 of the Courant limit [6].

For the TEM propagation frequency range, it can be seen from Fig. 1 that for dense grids (cell size $= \lambda_{\max}/10$; $\lambda_{\max}$ is the wavelength at the highest frequency of the excitation: $0.9f_c^{\mathrm{TM}_1}$ for TEM simulations, and $0.9f_c^{\mathrm{TM}_2}$ for TEM + TM$_1$ simulations), even eight PML cells offer a numerical reflection close to -80 dB for a theoretical reflection coefficient of 10^{-5}. Different values of theoretical maximum reflection ranging from 10^{-5} to 10^{-8} do not change significantly the numerical performance of the absorber (variation of 4–5 dB's). When 16 PML cells are used, the spurious reflection is below -100 dB for the whole frequency range. Similar conclusions can be drawn for the multimodal propagation (TEM + TM$_1$) in Fig. 2. It can be observed that 8 and 16 PML cells cause a numerical reflection close to -70 dB and below -100 dB, respectively. For coarse grids with cell sizes close to the Nyquist limit (cell size $= \lambda_{\max}/2.5$), the behavior of the PML layer changes. The large cell size causes retrospective reflections between the lossy cells and the numerical reflections from the absorber increase. Thus, a larger number of cells is required to obtain an acceptable reflection coefficient. Figs. 3 and 4 show that at least 32 cells are

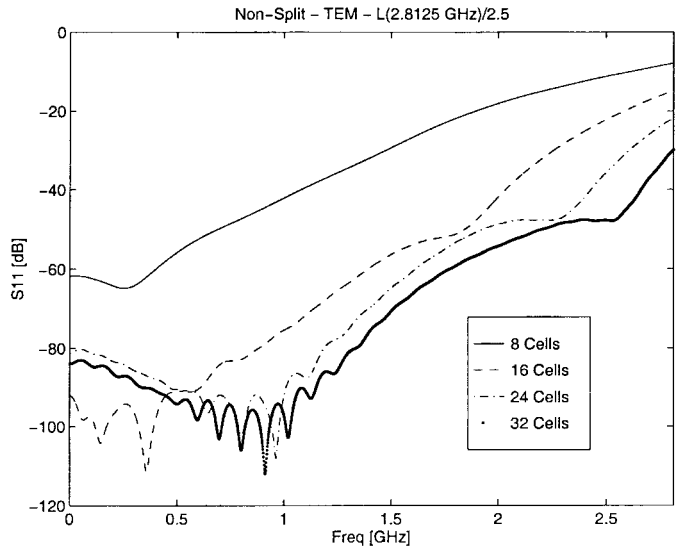

Fig. 3. TEM propagation—coarse grid.

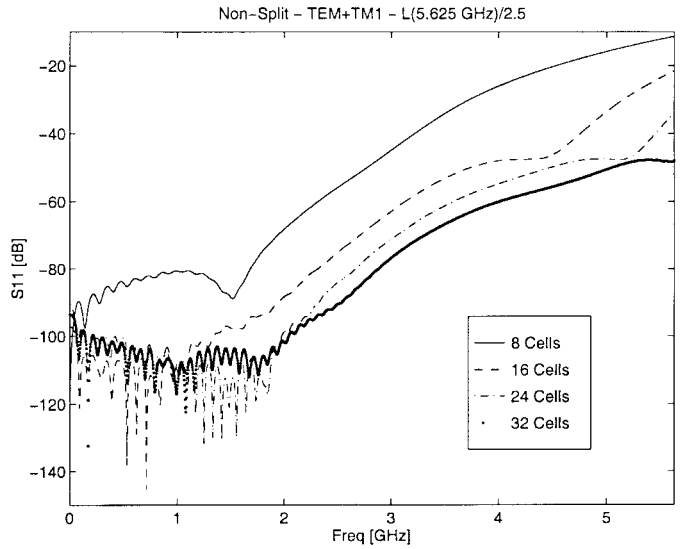

Fig. 4. Multimodal propagation—coarse grid.

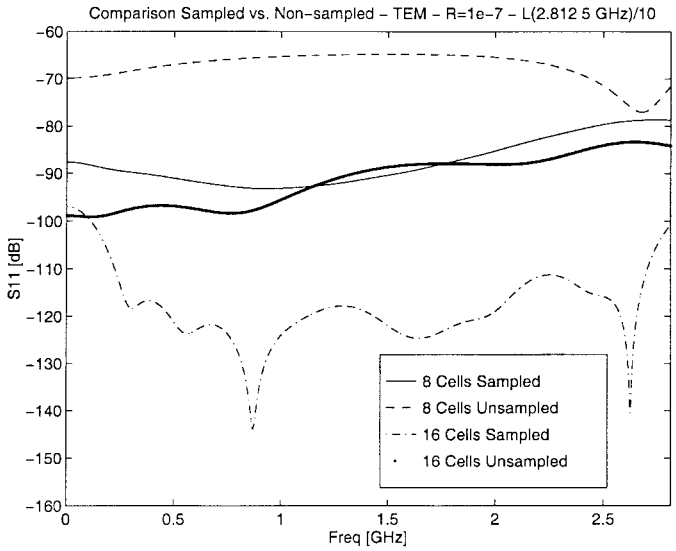

Fig. 5. Comparison of sampled versus nonsampled PML.

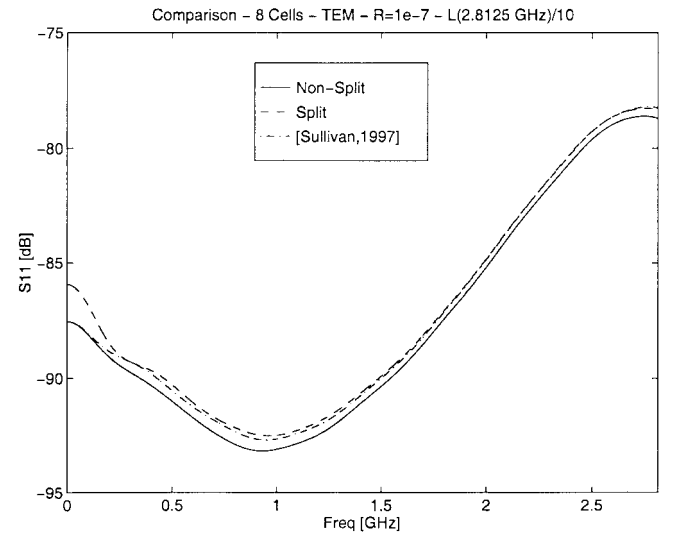

Fig. 6. Comparison of the split and nonsplit formulations with a recently proposed nonsplit PML algorithm.

needed for reflection around -50 dB for the high frequencies. Again, the reflection at lower frequencies is negligible (below -100 dB's). It should be emphasized that the loss coefficients assigned to each cell must be given by (15); that implies that the conductivity profile must be sampled with the scaling and wavelet functions that have a significant value in the PML layer. For all simulations, scaling (and wavelet) functions located up to six cells away from the PML layer are used for the sampling. When this procedure is not applied and the loss coefficients get the point value of the loss distribution at each cell (FDTD approach), the PML performance gets worse as it is displayed in Fig. 5.

It should be noted that the performances of the split and the nonsplit formulations are almost identical as it is displayed in Fig. 6. Recently, numerous nonsplit PML formulations have been proposed. All of them require the storage of extra variables, adding a significant memory overhead. The advantage of the proposed PML nonsplit formulation is that it doesn't require the update or storage of any additional variables, while maintaining a similar performance to other existing nonsplit formulations [7] as it is shown in Fig. 6. This formulation can be easily extended to other entire domain basis finite-difference schemes by simply adjusting the $a(i)$ coefficients of (14) and (21) as well as to schemes containing scaling and wavelet functions. In addition, it can be applied to the conventional FDTD scheme by replacing the summations of (14) and (21) with finite differences.

IV. Application of PML to the Analysis of Open Stripline Geometries

The PML nonsplit algorithm presented in Section III-B can be easily extended for the 2.5-D [2] and the 3-D MRTD algorithms incorporating scaling and wavelet functions maintaining the same performance characteristics. For each resolution added to the scheme, the conductivity must be sampled with

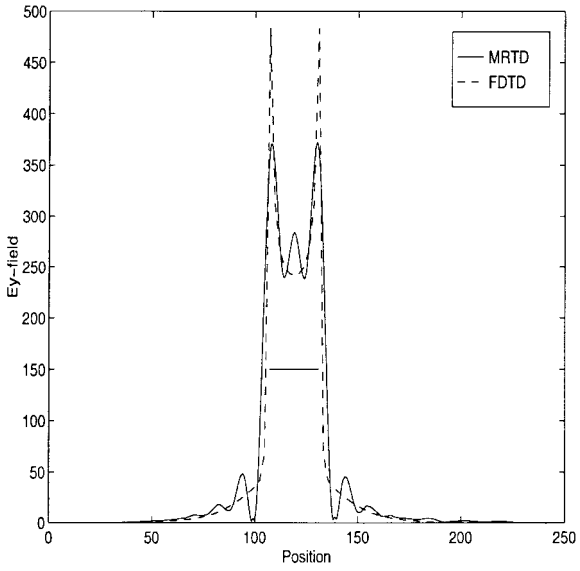

Fig. 7. Open single stripline—E_y TEM distribution.

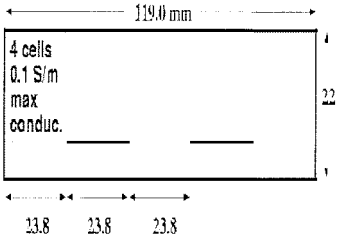

Fig. 8. Open-coupled stripline geometry.

an appropriately positioned wavelet function. It was observed that S_{11} changes only by 1–1.6 dB after the enhancement of multiple resolutions. In this section, the 2.5-D MRTD scheme is applied to the analysis of open single and coupled striplines to investigate propagation and coupling effects. In all simulations only wavelets of the zero resolution are used for both directions since the value of the higher resolution fields is negligible (smaller than 1%).

First, the 2.5-D MRTD scheme is applied to the analysis of the open stripline for the first (quasi-TEM) propagating mode. The analysis for the higher order propagating modes is straightforward. The central strip has a length of 23.8 mm and the distances from the top and bottom are 5.5 and 16.5 mm, respectively. The structure is filled with air ($\epsilon_r = 1.$). The PML absorber is applied for four cells to the left and the right sides of the structure and the maximum conductivity is $\sigma_E^m = 0.1$ S/m. For the analysis using Yee's FDTD scheme, a 42×28 mesh is used resulting in a total number of 1176 grid points. Analyzing the structure with the 2-D MRTD scheme, a mesh 12×4 (48 grid points) is chosen to reduce the total number of grid points by a factor of 24.5. In addition, the execution time for the analysis is reduced by a factor of four to five. The time discretization interval is chosen to be identical for both schemes and equal to 1/10 of the 2-D MRTD maximum Δt. For the analysis $\beta = 30$ is used and 20 000 time-steps are considered. From Table I it can observed that the calculated frequencies of the dominant propagating mode for $\beta = 30$ by use of 2-D MRTD scheme is very close to the theoretical values since the largest error is less than 0.1%, for mesh sizes much smaller than those used for the conventional FDTD simulations.

TABLE I
DOMINANT MODE FREQUENCY FOR $\beta = 30$

Mode	TEM	Rel.Error
Analytic values	1.4324 GHz	0.000%
12x4 MRTD	1.4329 GHz	0.035%
12x8 MRTD	1.4325 GHz	0.007%
42x28 FDTD	1.4321 GHZ	-0.021%

TABLE II
Z_o FOR DIFFERENT MESH SIZES

	Z_o (Ω)	Relative error
Analyt. Value	56.83	0.0%
12x4 MRTD	57.24	+0.72%
12x8 MRTD	57.09	+0.46%
42x28 FDTD	54.96	-3.29%

In Fig. 7, the pattern of the E_y field just below the strip has been calculated and plotted by use of the 2-D MRTD scheme. The pattern obtained by use of the conventional FDTD scheme is plotted for comparison. Since the edge effect is prominent, a mesh 12×8 (96 grid points) with scaling functions and wavelets of zero resolution is used for the MRTD simulation.

For the FDTD summations, only one field value per cell is needed due to the fact that pulse expansion functions that are constant for each cell are utilized. On the contrary, for the 2-D MRTD summation the field values for a number of subpoints along the integration path have to be calculated since the expansion functions are not constant for each cell. Table II shows the calculated values of the characteristic impedance Z_o [8]. It has been observed that the accuracy of the calculation of the characteristic impedance is improved by increasing the number of subpoints per cell at which the field values are calculated. An accuracy better than 1% is achieved if the field values are computed for more than nine subpoints per cell along the integration path. The characteristic impedance Z_o values for the TEM mode of the stripline listed on this table are computed from

$$Z_o = \frac{V}{I} = \frac{\int_{C_v} E_y \, dy}{\oint_{C_c} H dl} \tag{22}$$

where the integration paths C_v is a line from the stripline to the ground plane and C_c is a closed loop around the stripline. Since both of the schemes used in the analysis are discrete in space domain, the above integrals are transformed to summations.

A similar procedure was used for the analysis of the open-coupled stripline geometry of Fig. 8 for the dominant even and odd modes. Both strips have a length of 23.8 mm, the distances between them is 23.8 mm from the top PEC 16.5 mm and from the bottom PEC 5.5 mm. The MRTD-PML layer has a thickness of four cells (23.8 mm) with maximum conductivity

TABLE III
PML LAYER PARAMETERS

	PML cells along x + y	PML cells along z	R (Eq. 6)
FDTD ($60 \times 100 \times 16$)	6	6	$1 \cdot 10^{-6}$
MRTD($30 \times 50 \times 9$)	6	2–6	$1 \cdot 10^{-6}$
MRTD ($20 \times 20 \times 9$)	6	6–10	$1 \cdot 10^{-6}$

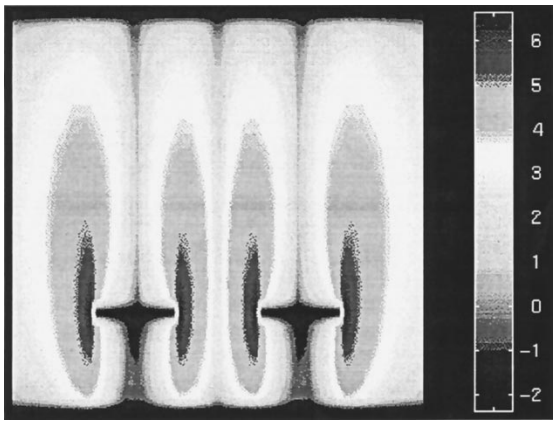

Fig. 9. Tangential E-field distribution (open–even mode).

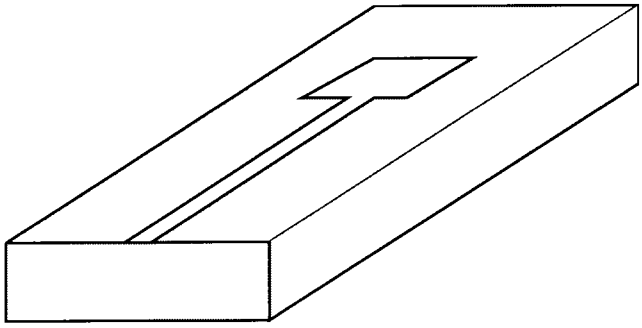

Fig. 10. Patch antenna geometry.

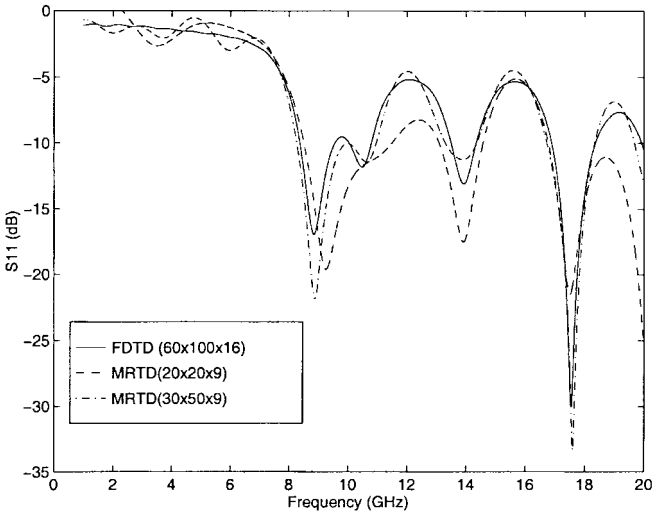

Fig. 11. S_{11} comparison plots for a patch antenna.

0.1 S/m and starts *exactly* at the edge of the striplines. The structure is filled with air ($\epsilon_r = 1$). For the analysis with the conventional FDTD scheme, a 65 $\times$ 20 mesh resulted in a total number of 1300 grid points. The same accuracy is achieved by an MRTD mesh 20 $\times$ 4 (80 grid points) resulting in an economy of memory by a factor of 16.25. The space distribution of the tangential-to-stripline E is plotted in logarithmic scale in Fig. 9 for the even mode. The agreement with the field distribution that is obtained with FDTD is very good, something that proves that MRTD provides accurate results in microscopic (field distribution) and macroscopic (Z_o) parameters.

V. APPLICATION OF PML TO A 3-D ANTENNA STRUCTURE

MRTD can successfully model both planar circuits [2] and resonating structures [9]. Recently, the techniques developed for the simulation of both structures are combined to model a 3-D patch antenna geometry [10]. Full 3-D MRTD analysis is used with PML expanded through three coordinate directions. The procedure to derive an equation for the 3-D MRTD scheme, with PML along all three coordinate directions is presented in [10].

The patch antenna (Fig. 10) used in our simulations has the dimensions 12.45 mm $\times$ 16 mm, with a microstrip line 20 mm long used as a feed. A Gaussian pulse 4 mm from the PML layer is used to excite the microstrip. The substrate has a thickness of 0.794 mm and a relative dielectric constant equal to one. An FDTD mesh of 60 $\times$ 100 $\times$ 16 is compared to MRTD grids of 30 $\times$ 50 $\times$ 9 and 20 $\times$ 20 $\times$ 9, which exhibit savings of memory over FDTD on the order of 7.22 and 33, respectively. Note that these values do not include the PML layers. The time discretization interval used for the MRTD 30 $\times$ 50 $\times$ 9 scheme is $\Delta t = 1.4008 \cdot 10^{-13}$ s while the MRTD 20 $\times$ 20 $\times$ 9 scheme uses a time discretization interval of $\Delta t = 1.42384 \cdot 10^{-13}$ s. FDTD uses a time discretization interval of $\Delta t = 1.4237 \cdot 10^{-13}$ s. In all three cases the simulation is performed for 10 000 time steps. Information for the PML layer is summarized in Table III.

Fig. 11 shows a comparison between S_{11} values for each of the three cases seen in Table III and exhibits a high degree of correlation between the methods, even with MRTD at low discretization. Six cells of PML terminate the computational domain along the $\pm x$, $\pm y$, and $+z$ directions with $\sigma_{\max}^{Ex} = \sigma_{\max}^{Ey} = 3.0$ and $\sigma_{\max}^{Ez} = 11.53$ for all cases. The higher low-frequency ripple of the MRTD results can be eliminated by using more PML cells. It has been observed that 10 PML cells achieve a ripple similar to that of the FDTD technique. Again, planar distributions of the E_z (vertically directed E-field component, probed just underneath the microstrip), calculated with FDTD (grid: 60 $\times$ 100 $\times$ 16) and MRTD (grid: 20 $\times$ 20 $\times$ 9) show very good agreement, though the MRTD grid requires

27 times less cells. Further economies can be obtained with thresholded use of zero-resolution space wavelets [4], while the PML exhibits satisfactory performance for both scaling and wavelet coefficients.

VI. Conclusion

A nonsplit and a split PML formulation for MRTD in 2-D has been derived and validated. The numerical performance is investigated for a different number of cells, theoretical reflections and cell-sizes and conclusions concerning the appropriate parameters have been drawn. The development of the MRTD-PML absorber enhances the applicability of the MRTD technique to complex 3-D open geometries while maintaining the high computational efficiency in terms of memory and execution time requirements.

References

[1] M. Krumpholz and L. P. B. Katehi, "MRTD: New time domain schemes based on multiresolution analysis," *IEEE Trans. Microwave Theory Tech.*, vol. 44, pp. 555–561, Apr. 1996.
[2] E. M. Tentzeris, R. L. Robertson, M. Krumpholz, and L. P. B. Katehi, "Application of MRTD to printed transmission lines," in *Proc. Microwave Theory Tech. Soc.*, 1996, pp. 573–576.
[3] M. Krumpholz and L. P. B. Katehi, "MRTD modeling of nonlinear pulse propagation," *IEEE Trans. Microwave Theory Tech.*, to be published.
[4] E. Tentzeris, R. Robertson, A. Cangellaris, and L. P. B. Katehi, "Space- and time-adaptive gridding using MRTD," in *Proc. Microwave Theory Tech. Soc.*, Denver, CO, 1997, pp. 337–340.
[5] J.-P. Berenger, "A perfectly matched layer for the absorption of electromagnetic waves," *J. Comput. Phys.*, vol. 114, pp. 185–200, 1994.
[6] E. Tentzeris, R. Robertson, J. Harvey, and L. P. B. Katehi, "Stability and dispersion analysis of Battle–Lemarie based MRTD schemes," *IEEE Trans. Microwave Theory Tech.*, to be published.
[7] D. M. Sullivan, "An unsplit step 3-D PML for use with the FDTD method," *IEEE Microwave Guided Wave Lett.*, vol. 7, pp. 184–186, July 1997.
[8] B. C. Wadell, *Transmission Line Design Handbook.* Norwood, MA: Artech House, 1991, pp. 136–137.
[9] R. Robertson, E. Tentzeris, M. Krumpholz, and L. P. B. Katehi, "Application of MRTD analysis to dielectric cavity structures," in *Proc. Microwave Theory Tech. Soc.*, 1996, pp. 1840–1843.
[10] R. Robertson, E. Tentzeris, and L. P. B. Katehi, "Modeling of membrane patch antennas using MRTD analysis," in *Proc. Antennas Propagat. Soc.*, 1997, pp. 126–129.

Emmanouil M. Tentzeris (S'89–M'82) was born in Piraeus, Greece, in 1970. He received the electrical engineering and computer science diploma degree (*suma cum laude*) from the National Technical University of Athens (NTUA), Athens, Greece, in 1992, and the M.Sc. and Ph.D. degrees from the University of Michigan, Ann Arbor, in 1993 and 1998, respectively.

From 1992 to 1998, he was a Graduate Research Assistant at the Radiation Laboratory, University of Michigan, Ann Arbor. He is currently an Assistant Professor with the Electrical and Computer Engineering Department, Georgia Institute of Technology, Atlanta. He has authored or coauthored more than 35 papers in referred journals and conference proceedings. His research interests include the development of novel numerical techniques and the application of the principles of multiresolution analysis in the simulation of microwave circuits used in wireless or satellite communication systems.

Dr. Tentzeris is a member of the Technical Chamber of Greece. He was awarded the 1997 Best Paper Award presented by the International Microelectronics and Packaging Society.

Robert L. Robertson was born in Fairfax, VA, in 1971. He received the B.S.E.E. degree from the University of Wisconsin, Madison, in 1995, and the M.S.E.E. degree from the University of Michigan, Ann Arbor, in 1997. He is currently working toward the Ph.D. degree at the University of Michigan, Ann Arbor.

He is currently a Graduate Research Assistant with the Radiation Laboratory, University of Michigan, Ann Arbor. His research interests include the development of time-domain analysis techniques used in the analysis of antennas and wireless communication systems.

Mr. Robertson is a member of Eta Kappa Nu.

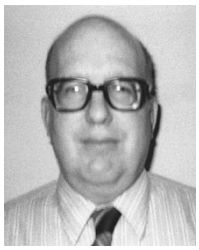

James F. Harvey (M'91) received the B.S. degree in engineering from the U.S. Military Academy, West Point, NY, in 1964, the M.A. in physics from Dartmouth College, Hanover, NH, in 1972, and the Ph.D. degree in applied science from the University of California at Davis, in 1990, with research performed at Lawrence Livermore National Laboratory.

He served in a variety of electrical engineering and research assignments as a member of the U.S. military before retiring. He is currently a civilian Research Program Manager at the Army Research Office, Research Triangle Park, NC, with primary responsibility for the fields of electromagnetics, antennas and antenna structures, innovative microwave and millimeter-wave circuit integration, low-power/minimum-power system design, and landmine detection. His programs include a focus on small multifrequency multifunctional antennas for army vehicles, radio propagation over complex terrain affecting data communications, and new millimeter-wave circuit integration techniques such as spatial power combining, micromachining, and advanced electromagnetic calculational techniques. His personal research interests are in the fields of quasi-optics, radio wave propagation, and multiresolution analysis of electromagnetic structures.

Dr. Harvey is an active member in the IEEE MTT Society, the IEEE AP Society, URSI Commission D, and SPIE. He is an organizer of the annual conference on the detection and remediation technologies for mines and mine-like targets in the SPIE Aerosense Meeting and is the editor of the conference proceedings. He received the Army R&D Award in 1992.

Linda P. B. Katehi (S'81–SM'85–F'95) received the B.S.E.E. degree from the National Technical University of Athens, Greece, in 1997, and the M.S.E.E. and Ph.D. degrees from the University of California, Los Angeles, in 1981 and 1984, respectively.

In September 1984, she joined the faculty of the Electrical Engineering and Computer Science Department, University of Michigan, Ann Arbor, where she is currently an Associate Dean of graduate education and Professor of electrical and engineering and computer science. She has been interested in the development and characterization (theoretical and experimental) of microwave, millimeter printed circuits, the computer-aided design of very large-scale integration (VLSI) interconnects, the development and characterization of micromachined circuits for millimeter-wave and submillimeter-wave applications, and the development of low-loss lines for terahertz-frequency applications. She has also been theoretically and experimentally studying various types of uniplanar radiating structures for hybrid-monolithic oscillator and mixer designs.

Dr. Katehi is a member of IEEE Antennas and Propagation Society and Microwave Theory and Techniques Society, Hybrid Microelectronis, URSI Commission D, and Sigma Xi. From 1992 to 1995 she was a member of the IEEE AP-S AdCom. She is an Associate Editor for the IEEE Transactions on Microwave Theory and Techniques. She was awarded the 1984 IEEE AP-S W. P. King Best Paper Award, the 1995 IEEE AP-S A. Schelkunoff Best Paper Award, the NSF Presidential Young Investigator Award, a 1987 URSI Young Scientist Fellowship, the Humboldt Research Award, the 1994 University of Michigan Faculty Recognition Award, and the 1996 IEEE MTT-S Microwave Prize.